Second order magnetic contributions to the hyperfine splitting of the $5snd\ ^1D_2$ states in ^{87}Sr.

J. Güdde, A. Klinkmüller *, P. J. West, and E. Matthias
Institut für Experimentalphysik, FU Berlin, Arnimallee 14, 1000 Berlin 33, Germany

20 January 1993

Abstract

The hyperfine structure of $5snd\ ^1D_2$ states in ^{87}Sr was studied for principal quantum numbers $11 \leq n \leq 25$ by Doppler-free two-photon excitation combined with thermionic detection. Based on the more accurate data, compared to previous results, the hyperfine structure was analysed by second order perturbation theory using MQDT wavefunctions. As a result we find that the surprisingly large B-factors obtained by fitting the data with the Casimir formula do not reflect a quadrupolar interaction but rather consist predominantly of second order magnetic dipole contributions. Further, inconsistencies in the King plot of odd-even isotope shifts were removed by this type of analysis. The result demonstrates the importance of higher order effects in hyperfine splittings of excited states in atoms with two valence electrons, even when the fine structure splitting is large compared to the hyperfine splitting.

PACS numbers: 35.10.Fk, 32.80.Rm, 31.30.Gs

1 Introduction

Many problems in atomic physics can be treated using perturbation theory. Normally for low lying states with large energy distances to neighbouring levels the application of perturbation theory in first order gives satisfying results. However, the level spacing of high lying states (Rydberg states) is considerably smaller and higher order perturbation theory is required for correct treatment.

The electron configuration of excited states of the alkaline earth elements is determined by the two electrons outside a core of closed electron shells. The existence of low lying bound doubly excited states causes configuration mixing and influences the coupling of the two valence electrons (singlet-triplet mixing). The multichannel quantum defect theory (MQDT) has proved to be an efficient tool [1] for the description of such perturbed Rydberg states with only a small set of parameters.

Particularly the atomic hyperfine structure (hfs) is sensitive to admixtures in the wave function of Rydberg states [2] and is therefore a most sensitive quantity for investigating such phenomena.

For the evaluation of the hfs it is in most cases sufficient to consider only the magnetic dipole and the electric quadrupole interaction. Then it is possible to parameterize the hfs – splitting in first order perturbation theory by the hyperfine constants A and B, using the Casimir formula. The hyperfine constants A and B measure the magnitude of the magnetic dipole and the electric quadrupole interaction, respectively. This kind of evaluation and separation of the interactions assumes that contributions of higher order perturbation theory are negligible. If that is not the case the hyperfine constants lose their physical meaning.

Previously, the effects of higher order contributions to the hfs in Rydberg states due to neighbouring fine structure levels have been observed in Hg [3–5],

*Göteborgs universitet and Chalmers tekniska högskola AB, Avd. för atomfysik, Fysikgränd 3, SE-412 96 Göteborg, Sweden

^{3}He [6], Ca [7], Sr [2, 7–10], Ba [2, 7, 11–15], Sm [16], Yb [18], and Pb [17]. For very high Rydberg states the energy spacing of states with different principal quantum number n is small enough to cause hyperfine induced mixing [19–21].

In the present work we report on high resolution laser spectroscopic measurements of the hfs of $5snd\ ^1D_2$ states in ^{87}Sr and of transition isotope shifts of the stable isotopes ^{84,86,88}Sr for principal quantum numbers $11 \leq n \leq 25$. These measurements were done with enhanced accuracy compared to previous results [22, 23], in order to obtain sufficiently precise data for accurate comparison of the hfs with the results derived from second order perturbation theory. The hfs was calculated by means of MQDT-wavefunctions in first and second order perturbation theory. We found that second order contributions need to be considered in the analysis of the hfs in order to explain the unexpected large hyperfine constant B and the shift of the hyperfine multiplet, which is responsible for large deviations from the linear dependence in a King Plot analysis.

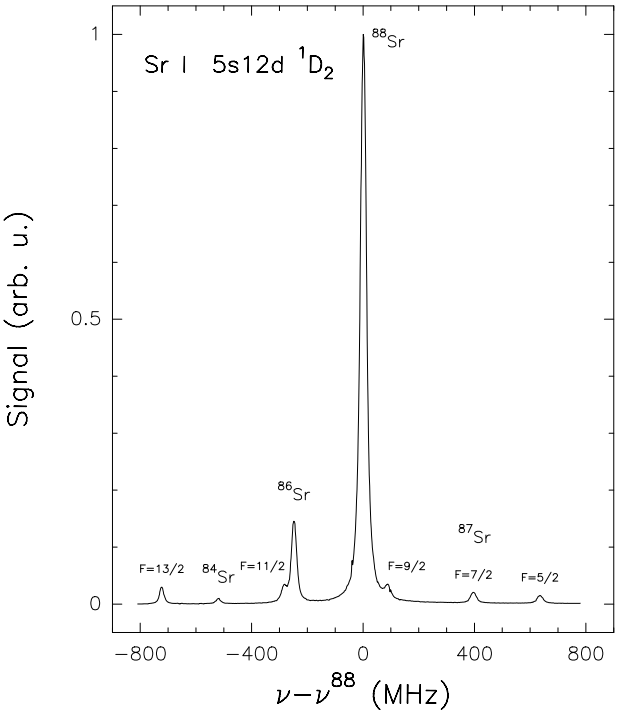

Figure 1: Two-photon excitation spectrum of the $5s^2\ ^1S_0 \rightarrow 5s12d\ ^1D_2$ transition as a function of the energy detuning relative to the signal of the isotope ^{88}Sr.

2 Experiment

The experimental set-up used in the present work has been described in detail in an earlier paper [24]. Briefly, it consisted of a cw narrow bandwidth ring dye laser (Spectra Physics Model 380D) pumped by an argon ion laser (Spectra Physics Model 2045). Typical operating conditions were uv pump powers of 2.5–3.0 W, resulting with a stilben 3 dye in 200–400 mW single-mode power. The dye laser is tunable between 410 and 470 nm. With these wavelengths Sr I Rydberg levels above $n = 8$ can be excited from the $5s^2\ ^1S_0$ ground state by Doppler-free two-photon excitation. A Michelson-type wave meter (Burleigh WA 20) with 300 MHz accuracy was used for identifying Rydberg levels up to $n = 200$. For measuring the hfs – splittings the laser frequency was stabilized to an external confocal cavity. This, in turn, was controlled by an active molecular frequency standard with an accuracy of better than 100 kHz, using several precisely known I_2 levels combined with the frequency-offset-locking technique [25]. A computer (HP 21 MX-E) was employed for real-time data acquisition and for scanning and controlling the laser frequency.

The Sr-atoms were excited and, following collisional ionization, detected with high efficiency in a thermionic ring diode [26]. In order to improve the signal to noise ratio, the retroreflected laser beam was chopped at a frequency of 80 Hz for lock-in detection (EG&G PAR Model 5210).

A typical spectrum of the $5s12d\ ^1D_2$ state is shown in Fig. 1. To determine the line positions, Lorentzian line profiles were fitted to the experimental data. The accuracy of the line distances was enhanced by recording and evaluating several spectra (up to 40) for each state. The mean values of the transition frequency differences with regard to ^{88}Sr are listed in Table 3.

3 Theory of hyperfine structure

The hyperfine interaction describes the interaction between the electrons and the magnetic and electric multipole moments of the nucleus, where the even magnetic and the odd electric multipole moments vanish. In most cases it is sufficient to take into account only the interaction with the nuclear magnetic dipole moment $\boldsymbol{\mu}_I = g_I \mathbf{I}$ and the electric quadrupole moment $\mathbf{Q}$. According to Sobel'man [27], the Hamiltonian can than be expressed as

$$H_{\mathrm{hfs}} = H_\mu + H_Q \ , \tag{1}$$

where

$$\begin{aligned} H_\mu = \sum_i [a_{\ell_i} (\boldsymbol{\ell}^{(1)} - \sqrt{10}[\mathbf{s}^{(1)} \times \mathbf{C}^{(2)})]^{(1)}) \\ + a_{s_i} \delta_{\ell_i,0} \mathbf{s}^{(1)}] \cdot \mathbf{I}^{(1)} \quad , \end{aligned} \tag{2}$$

$$H_Q = -e^2 \sum_i {r_i}^{-3} \mathbf{C}^{(2)} \cdot \mathbf{Q}^{(2)} \ , \tag{3}$$

and $\boldsymbol{\ell}^{(1)}$ and $\mathbf{s}^{(1)}$ are the single electron angular momentum and spin operators, respectively. The tensor $\mathbf{C}^{(2)}$ is connected to the spherical harmonics $Y_{\ell m}$ by $C^\ell_m = [4\pi/(2\ell+1)]^{1/2} Y_{\ell m}$.

In first order perturbation theory the hyperfine interaction yields an energy splitting

$$\Delta E^{(1)}_F = \langle \gamma J I F | H_{\mathrm{hfs}} | \gamma J I F \rangle \tag{4}$$

of a state with total angular momentum $\mathbf{F} = \mathbf{I} + \mathbf{J}$. Here $\mathbf{I}$ and $\mathbf{J}$ are the angular momenta of the nucleus and the electrons, respectively. Evaluating this matrix element, one obtains the well known Casimir formula [28]

$$\Delta E^{(1)}_F = \frac{1}{2} AK + B \frac{\frac{3}{4} K(K+1) - J(J+1) I(I+1)}{2I(2I-1)J(2J-1)} \ , \tag{5}$$

where

$$K = F(F+1) - J(J+1) - I(I+1) \ . \tag{6}$$

The hfs constants A and B describe the magnitudes of the magnetic dipole and electric quadrupole interactions, respectively. Due to the different dependence on F of the two terms in Eq. (5), it is possible to fit the Casimir formula to experimentally determined hfs – splittings, and to separate the contributions of the magnetic dipole and the electric quadrupole interaction.

The measurement of the isotope shift (IS) is also possible since for first order perturbation theory the center of gravity of a hyperfine multiplet remains unshifted ($\sum_F \Delta E^{(1)}_F (2F+1) = 0$).

The situation changes if one considers contributions of second order perturbation theory. The second order energy splitting of a state $|\gamma J I F\rangle$ is

$$\Delta E^{(2)}_F = \sum_{\gamma' J' \neq \gamma J} \frac{|\langle \gamma J I F | H_{\mathrm{hfs}} | \gamma' J' I F \rangle|^2}{(E_{\gamma J} - E_{\gamma' J'})} \ . \tag{7}$$

Hence when second order effects are not negligible, i.e. when neighbouring fine structure levels with equal quantum number F are lying close together, the energy splitting can no longer be approximated by the Casimir formula. Then it is not possible to separate magnetic dipole and electric quadrupole contributions from the experimental hfs – splittings, because the second order contribution of the magnetic dipole interaction has a similar dependence on F as the first order contribution of the electric quadrupole interaction. This is especially important when the hfs is dominated by the magnetic dipole interaction.

The second order energy splitting goes together with a shift of the center of gravity, since the contribution of each fine structure level has a different F dependence (only states with equal F are connected). This has the consequence that the IS of a perturbed hyperfine multiplet can only be extracted using second order perturbation theory.

To study the influence of the second order contributions, one can calculate the hfs in first and second order perturbation theory if the fine structure splitting is known. For a two electron atom like Strontium the magnetic dipole and electric quadrupole interaction can be written in terms of the one electron matrix elements $\langle a_\ell \rangle$ and $\langle b_\ell \rangle$. This has been worked out by Lurio *et al.* [29] for a $s\ell$-configuration. Explicit

expressions for a more general $\ell_1\ell_2$-configuration are given in the Appendix of the present work. The one electron matrix elements depend on the expectation value of r^{-3} for $\ell \neq 0$ and on the probability density at the nucleus, $|\psi(0)|^2$, for s-electrons. According to Sobel'man [27] $\langle a_\ell \rangle$ and $\langle b_\ell \rangle$ can be written in units of 1 Rydberg (R_∞) as :

$$\langle a_{\ell\neq 0}\rangle = g_I \alpha^2 \frac{m}{m_p} \langle R_{n\ell}| \frac{a_0^3}{r^3} |R_{n\ell}\rangle R_\infty \tag{8}$$

$$\langle b_{\ell\neq 0}\rangle = 2\frac{Q}{a_0^2} \langle R_{n\ell}| \frac{a_0^3}{r^3} |R_{n\ell}\rangle R_\infty \tag{9}$$

$$\langle a_{\ell=0}\rangle = \frac{8\pi}{3} \alpha^2 g_I \frac{m}{m_p} a_0^3 |\psi(0)|^2 R_\infty \tag{10}$$

$$\langle b_{\ell=0}\rangle = 0\ . \tag{11}$$

Here g_I is the nuclear g-factor, α the fine structure constant, m/m_p the ratio of electron and proton mass, e the elementary charge, $R_{n\ell}$ the radial part of the one-electron wavefunction and a_0 the Bohr radius. To a first approximation, $\langle R_{n\ell}|a_0^3/r^3|R_{n\ell}\rangle$ and $|\psi(0)|^2$ can be calculated using the formula from Ref. [27] :

$$\begin{aligned}\langle R_{n\ell}| \frac{a_0^3}{r^3} |R_{n\ell}\rangle &= \frac{1}{\ell(\ell+1)(\ell+\frac{1}{2})} \frac{Z}{n^{*3}} \\ &= \frac{1}{\ell(\ell+1)(\ell+\frac{1}{2})} \left(\frac{\epsilon_{n\ell}}{R_\infty}\right)^{3/2} \end{aligned} \tag{12}$$

$$|\psi(0)|^2 = \frac{1}{\pi a_0^3} \frac{Z}{n^{*3}} = \frac{1}{\pi a_0^3} \left(\frac{\epsilon_{ns}}{R_\infty}\right)^{3/2}\ , \tag{13}$$

where n^{*3} is the effective principal quantum number, $\epsilon_{n\ell}$ the binding energy (in Rydbergs) of the nl orbital, and Z the effective nuclear charge.

4 Calculation of the hyperfine splitting with MQDT wavefunctions

As shown in reference [1], the MQDT is a powerful tool to describe perturbed Rydberg series of alkaline-earth atoms.

The empirical MQDT study by Esherick [30] showed that the $J = 2$ bound-state spectrum of Strontium can be described by a five channel MQDT model which includes the recoupling of $^1D_2$ and $^3D_2$ channels and the perturbation of the $5snd\ ^1D_2$ and $^3D_2$ series by the $4dn's\ ^1D_2$, $4dn's\ ^3D_2$ and $5pn''p\ ^1D_2$ channels. Here, n' and n'' are the principal quantum numbers of the Rydberg series converging to the $4d$ and $5p$ ionization limits. Within the accuracy of that analysis it was found that it is not necessary to include the $4dn'''d\ ^1D_2$ channel.

Since there are only a few doubly-excited states below the first ionization limit, the empirical MQDT study cannot give the exact admixture of each doubly excited channel to the levels although the total amount of the doubly-excited channels can be well distinguished from the singly-excited ones. In particular Esherick's analysis can not be used to distinguish between the $5pn''p\ ^1D_2$ and $4dn'''d\ ^1D_2$ channels. On the other hand, MCHF calculations performed by Aspect *et al.* [31] and *ab initio* MQDT calculations of Aymar *et al.* [32] indicate that the $4dn'''d$ component is twice as large as the $5pn''p$ one. Thus the wavefunction of the even $J = 2$ bound states of Sr can be written as an expansion of pure LS states with the following terms

$$\begin{aligned}|\gamma J = 2\rangle = {} & z_1 |5snd\ ^1D_2\rangle_{LS} + z_2 |5snd\ ^3D_2\rangle_{LS} \\ & + z_3 |4dn's\ ^1D_2\rangle_{LS} + z_4 |4dn's\ ^3D_2\rangle_{LS} \\ & + z_5 \Big(\sqrt{\frac{1}{3}} |5pn''p\ ^1D_2\rangle_{LS} \\ & + \sqrt{\frac{2}{3}} |4dn'''d\ ^1D_2\rangle_{LS} \Big)\ ,\end{aligned}$$

where the z_i are the mixing coefficients obtained by using Esherick's [30] MQDT parameter. The mixing coefficients for the $5snd\ ^1D_2$ and $5snd\ ^3D_2$ states are drawn in Figs. 2 and 3 for principal quantum numbers $11 \leq n \leq 25$. The data show a strong singlet-triplet mixing in the $5snd$ configuration around $n = 16$. The main contribution of the doubly excited channels in this region of principal quantum numbers comes from the $4dn's$ configuration, where also a singlet-triplet mixing occurs.

As studied earlier [22], the hfs of the $5snd\ ^1D_2$ and

$^3D_2$ states is dominated by the Fermi-contact term of the magnetic dipole interaction of the $5s$ electron and depends strongly on the mixing coefficients z_1 and z_2. The $n\ell$ Rydberg electron has only a weak interaction with the nucleus. For pure $5snd\ ^1D_2$ Rydberg states the hfs – splitting should almost vanish and for pure $5snd\ ^3D_2$ the dipole constant A should be nearly $a_{5s}/12$. Only a weak quadrupole interaction due to the small admixtures of doubly excited channels is expected.

In the calculation of the hyperfine splitting of the $5snd\ ^1D_2$ states in second order pertubation theory states of different J and equal F enter the matrix elements (cf. Eq. 7). These are the fine structure levels $5snd\ ^3D_1$, $^3D_2$, and $^3D_3$ whereas the $5snd\ ^1D_2$ and $^3D_2$ states are described by Eq. 14, the expansion of the $5snd\ ^3D_1$ and $5snd\ ^3D_3$ states are taken from the two channel MQDT analysis given in Ref. [34] in which the mixing of the $5snd$ and $4dn's$ configuration have been considered. Thus the wavefunctions of the $J = 1$ and $J = 3$ states can be written as:

$$|\gamma J = 1\rangle = \alpha_1 |5snd\,^3D_1\rangle_{LS} + \alpha_2 |4dn's\,^3D_1\rangle_{LS} \quad (14)$$

$$|\gamma J = 3\rangle = \beta_1 |5snd\,^3D_3\rangle_{LS} + \beta_2 |4dn's\,^3D_3\rangle_{LS} \quad (15)$$

The mixing coefficients α_i and β_i can be calculated with the MQDT parameters given in Ref. [34].

The evaluation of the matrix elements is done here without considering matrix elements between different configurations $\ell_1\ell_2$. This is a reliable procedure because these matrix elements vanish in most cases, especially for the Fermi-contact term, or are very small due to the different effective quantum numbers. However, in special situations [33] the off-diagonal configuration matrix elements can be quit large.

Further the energy differences between the $5snd\ ^1D_2$ states and the other fine structure terms are needed for the calculations. These are listed in Table 1 and illustrated in Fig. 4. It can be seen that the energy differences of the three fine structure terms change their sign at different principal quantum numbers. As studied earlier [10], the small difference between the $5snd\ ^1D_2$ and $5snd\ ^3D_3$ series at $n = 19$ results in a large shift of the respective hyperfine multiplets.

In the calculation of the one-electron matrix ele-

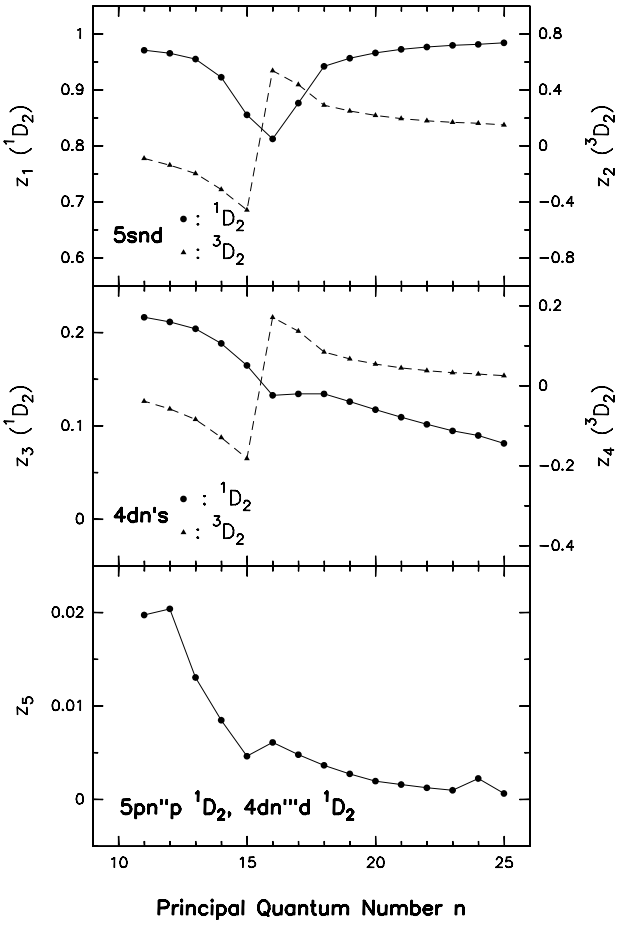

Figure 2: Admixtures of the pure LS-states according to Eq. 14 to the $5snd\ ^1D_2$ Rydberg serie of Strontium calculated with the MQDT-parameters from Ref. [30] as a function of the principal quantum number n.

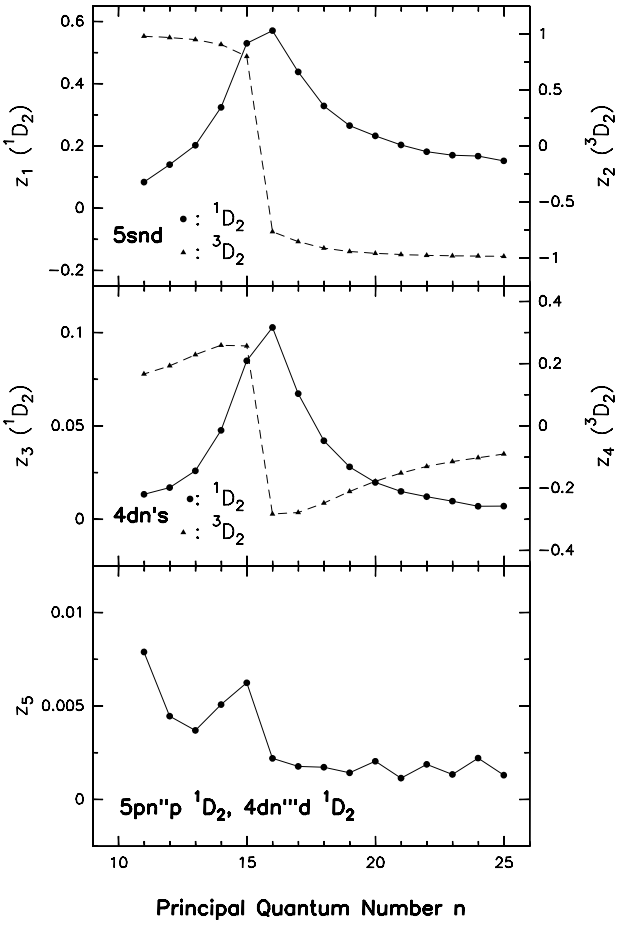

Figure 3: Admixtures of the pure LS-states according to Eq. 14 to the *5snd* $^3D_2$ Rydberg serie of Strontium calculated with the MQDT-parameters from Ref. [30] as a function of the principal quantum number n.

Table 1: Level energies of bound $5snd$ $^1D_2$, $^3D_1$, $^3D_2$ and $^3D_3$ states of Sr I (cf. Fig. 4.

	$^1D_2$	$^3D_1$	$^3D_2$	$^3D_3$
n	E (cm^{-1})	E (cm^{-1})	E (cm^{-1})	E (cm^{-1})
11	44578.6890[a]	44616.05[c]	44620.08[d]	44625.1[e]
12	44829.6648[a]	44854.02[b]	44860.06[b]	44865.22[b]
13	45012.0249[a]	45028.55[b]	45036.95[b]	45043.79[b]
14	45153.2785[a]	45159.60[b]	45171.49[b]	45180.44[b]
15	45263.6196[a]	45260.84[b]	45276.65[b]	45286.53[b]
16	45362.1272[a]	45341.36[b]	45350.35[b]	45370.76[b]
17	45433.2717[a]	45414.43[b]	45420.84[b]	45439.08[b]
18	45492.6101[a]	45475.35[b]	45479.88[b]	45495.02[b]
19	45542.2955[a]	45527.10[b]	45530.18[b]	45542.23[b]
20	45584.1831[a]	45570.97[b]	45573.28[b]	45582.38[b]
21	45619.7872[a]	45608.37[b]	45610.07[b]	45616.80[b]
22	45650.2617[a]	45640.43[b]	45641.68[b]	45647.54[b]
23	45676.5325[a]	45668.11[b]	45669.06[b]	45673.10[b]
24	45699.3308[a]	45692.08[b]	45692.90[b]	45695.94[b]
25	45719.2336[a]	45712.94[b]	45713.50[b]	45715.80[b]

[a]Reference [35].
[b]Reference [36].
[c]Calculated value from reference [37].
[d]Reference [30].
[e]Reference [38].

ments, the experimental value of $-1001(2)$ MHz from Ref. [39] was taken as a_{5s}-factor. The other one-electron matrix elements can be well approximated by introducing a_{5s}, and substituting Eqs. (12) and (13) into Eqs. (8) to (10) :

$$\langle a_{\ell\neq 0}\rangle = \frac{3}{8}\frac{a_{5s}}{\ell(\ell+1)(\ell+\frac{1}{2})}\left(\frac{\epsilon_{n\ell}}{\epsilon_{5s}}\right)^{3/2} \tag{16}$$

$$\langle a_{ns}\rangle = a_{5s}\left(\frac{\epsilon_{ns}}{\epsilon_{5s}}\right)^{3/2} \tag{17}$$

$$\langle b_{\ell\neq 0}\rangle = \frac{3}{4}\frac{Q}{a_0^2}\frac{a_{5s}}{\alpha^2 g_I \frac{m}{m_p}}\frac{1}{\ell(\ell+1)(\ell+\frac{1}{2})}\left(\frac{\epsilon_{n\ell}}{\epsilon_{5s}}\right)^{3/2} \tag{18}$$

According to MQDT, the binding energies of the $5s$, $5p$ and $4d$ orbitals are assumed to be the same as those of the corresponding $5s$, $5p$ and $4d$ orbitals in Sr^+. The additional binding energy of the nd, $n's$,

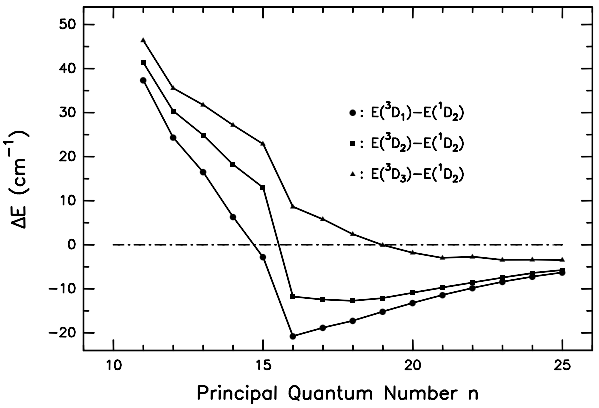

Figure 4: n dependence of the energy differences between the *5snd* $^3D_{1,2,3}$ and the *5snd* $^1D_2$ states of Strontium.

$n''p$ or $n'''d$ electron in a state can be approximately obtained by subtracting the energy of the inner orbit (eg. $5s$) from the energy of the state $|\gamma J\rangle$. The energies of the $5s$, $5p$ and $4d$ orbits in Sr^+ were taken from Ref. [38], where the mean values of the fine structure components were used for the $5p$ and $4d$ orbits. For the quadrupole moment of ^{87}Sr, we used the value of $0.335(20)\cdot 10^{-28}\,\mathrm{m}^2$ from Ref. [40], and for the dipole moment $\mu_I = g_I I = -1.089299(1)\mu_N$ reported in Ref. [41]. The matrix elements in Eqs. (16) to (18) were then introduced into the expressions listed in the Appendix to yield the energy splittings.

The results of the calculations are shown in Fig. 5. The second order contributions of the electric quadrupole interaction are less than 1 kHz and will be neglected here. It should be emphasized here that the first order electric quadrupole contributions are approximately one hundred times smaller than the second order magnetic dipole contributions. The second order contribution of the magnetic dipole interaction in the $5s19d$ $^1D_2$ state is not shown here because of the small energy separation to the $5s19d$ $^3D_3$ state (≈ 2 GHz). In that particular case the contributions to the hfs are large in any higher order, which means that perturbation theory is not longer applicable. This is discussed in detail in Ref. [10].

Due to the strong Fermi-contact interaction of the $5s$ electron, the calculated total hfs – splittings for

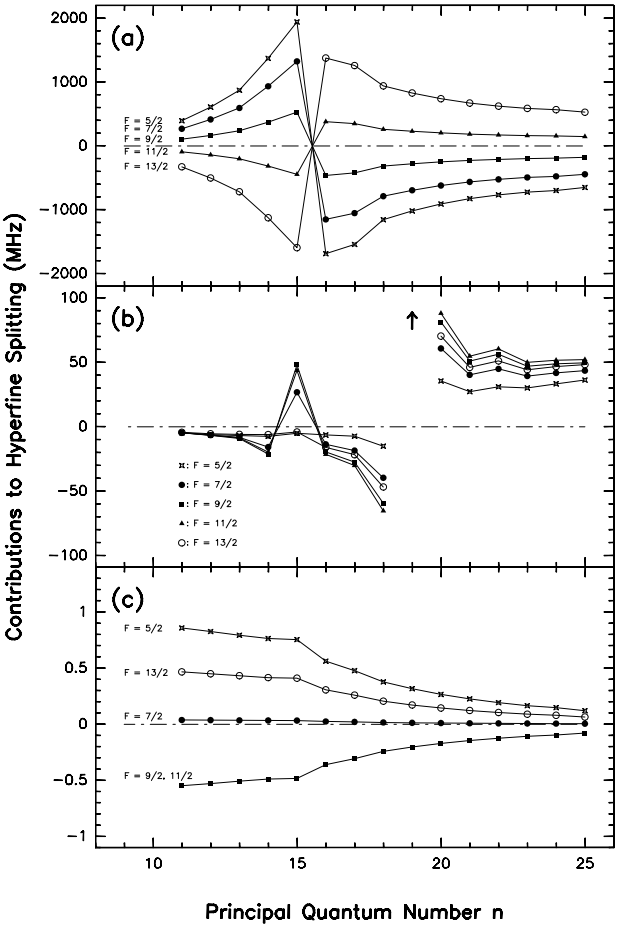

Figure 5: Calculated energy-contributions to the hyperfine splitting of the *5snd* $^1D_2$ states in ^{87}Sr as a function of n. (a) : magnetic dipole interaction in first order, (b) : magnetic dipole interaction in second order (the very large contribution of the *5s19d* $^1D_2$ is only indicated by the arrow and is discussed in detail in Ref. [10]), and (c) : electric quadrupole interaction in first order perturbation theory.

these states depend almost entirely on the mixing coefficients z_1 and z_2 and on the experimental value of the a_{5s}-factor.

5 Comparison with the experimental data

5.1 Hyperfine Splitting

In Fig. 6 the calculated hfs – splittings are compared with the experimental data. The isotope shifts of the experimental data are taken into account by shifting the centers of gravity of the calculated hyperfine multiplets to overlap with the experimental ones. Good agreement between experimental and theoretical data is achieved. The small deviations of the individual components can be explained by the fact, that the hfs is much more sensitive to the mixing parameters in the expansion of Eq. (14), especially to z_1 and z_2, than to the energies of the states which are used in the empirical MQDT analysis (see Ref. [42]). To emphasize this point we have done a least square fit of the theoretical line positions for each state by varying the center of gravity of the multiplet and the mixing coefficients z_1 and z_2 under the condition $z_1^2 + z_2^2 = constant$. With only small changes of the mixing coefficients, which cause large effects on the hfs splitting, one can obtain a perfect agreement between experimental and theoretical line positions, as is shown in Fig. 7. The optimized mixing coefficients differ very little from the MQDT mixing coefficients except near $n = 15$, as can be seen in Fig. 8 and Table 2. Therefore, in the following discussion it is sufficient to use the MQDT mixing coefficients for the description of the main features of the hfs splitting.

The need for considering second order effects for the hfs becomes evident, when one tries to separate the magnetic dipole and electric quadrupole contributions by fitting the Casimir formula (which contains only first order effects) to the measured and calculated hfs – splittings. This is shown in Fig. 9(a) and 9(b) and is listed in Table 4. At the first glance an excellent agreement between experiment and theory is obtained. However, the large constant B in Fig. 9(b) does not describe the electric quadrupole interaction,

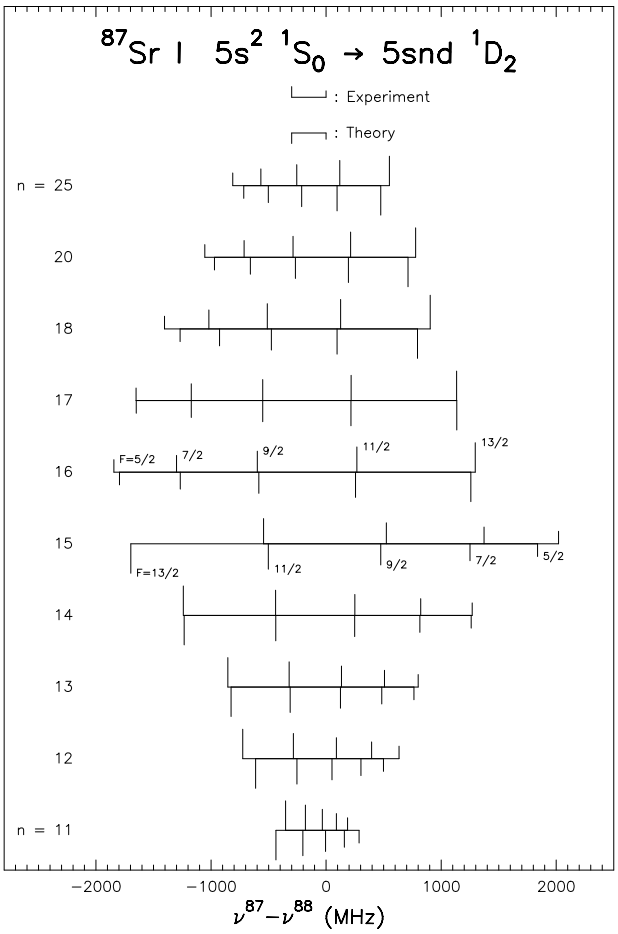

Figure 6: Comparison between the measured and calculated (in second order) hyperfine splitting of the *5snd* $^1D_2$ states in ^{87}Sr. The isotope shift is taken into account by shifting the centers of gravity of the calculated multiplets for agreement with the experimental ones.

and reflects mainly the second order contribution of the magnetic dipole interaction. The contribution of the quadrupole interaction is very small indeed, and is determined by the admixture of the $4dn's$ configuration. This is shown in Fig. 9(c), where the electric quadrupole interaction is considered to first order only.

5.2 Isotope Shift

The influence of the second order effects on the IS can be seen in a King-plot analysis in Fig. 10. The King-plot procedure (see Ref. [43]) can be used for testing the consistency of the IS measurement in two transitions. It allows the separation of the specific mass and the field shift of a transition, provided the specific mass and the field shift are known for a reference transition. In a King-plot, the modified IS $\xi_i^{A,A'}$ of a transition i between two isotopes with mass numbers A and A' (where $A' > A$) is plotted against the modified IS $\xi_j^{A,A'}$ of the reference transition. The modified IS is defined as the difference between the experimental IS $\delta\nu_i^{A,A'}$ and the normal mass shift multiplied by the factor $m_A m_{A'}/(m_{A'} - m_A)$, where m_A and $m_{A'}$ are the masses of the isotopes :

$$\xi_i^{A,A'} = \delta\nu_i^{A,A'} \frac{m_A m_{A'}}{m_{A'} - m_A} - m_e \nu_i \ . \qquad (19)$$

Here m_e is the electron mass and ν_i the transition energy. In a King-plot the points for different isotope pairs should lie on a straight line.

For the transitions $5s^2\ ^1S_0 \rightarrow 5snd\ ^1D_2$ in Sr I this is true only for the even isotope pairs. As an example, Fig. 10 shows a King-plot for the transition Sr I $5s^2\ ^1S_0 \rightarrow 5s17d\ ^1D_2$. The transition Sr II $5s\ ^2S_{1/2} \rightarrow 5p\ ^2P_{1/2}$ from Ref. [39] was taken as reference transition. Obviously the points involving the odd isotope ^{87}Sr (which are calculated using the center of gravity of the experimental hfs – splitting listed in Table 4) are far off the linear dependence of the even isotope pairs. This effect was also noticed in Ref. [18] for Ytterbium, where the deviation from a straight line was taken to determine the magnitude of the second order contributions. If one corrects the experimental IS of the ^{87}Sr for the second order contribution to the shift, represented by the center of

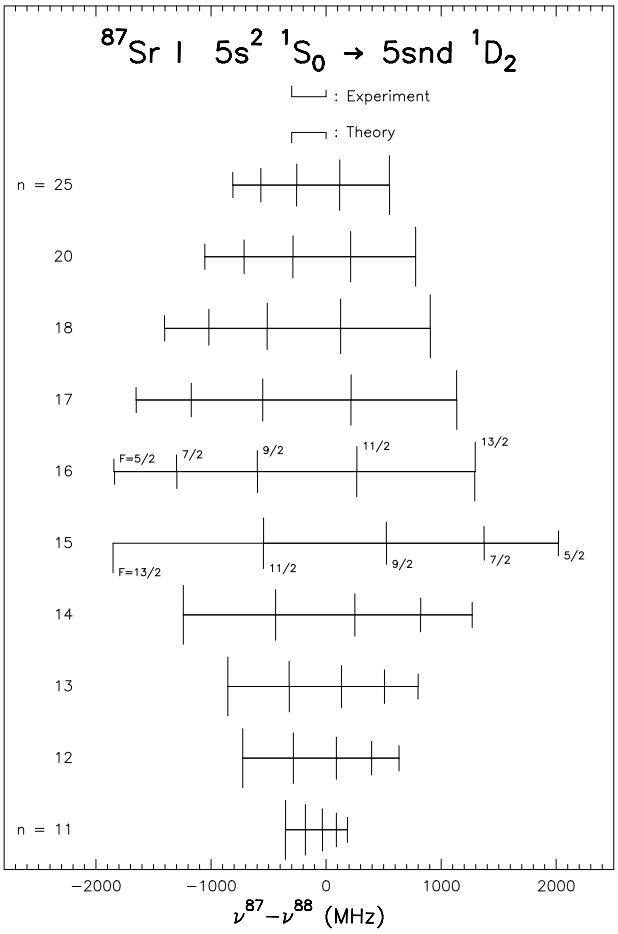

Figure 7: Comparison between the measured and calculated hyperfine splitting of the $5snd\ ^1D_2$ states in ^{87}Sr. Compared to Fig. 6 the theoretical line positions are optimized by a least square fit of the mixing coefficients z_1, z_2 and the center of gravity of the multiplet.

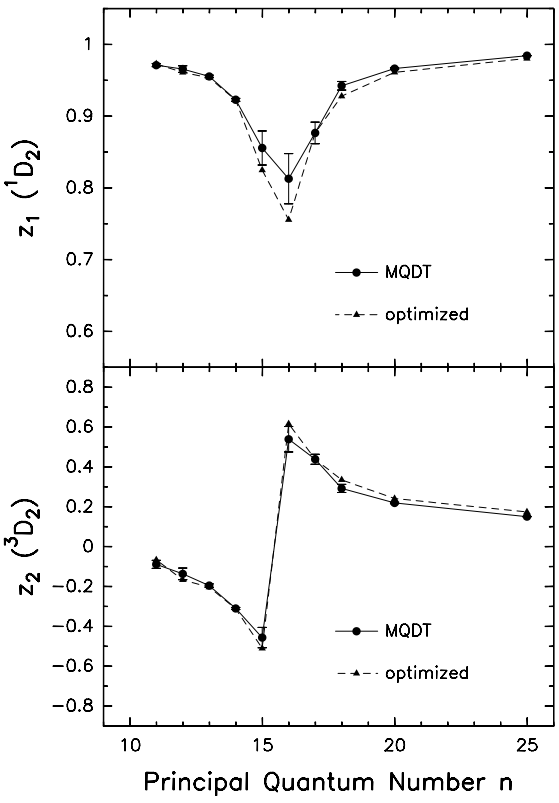

Figure 8: Comparison between the mixing coefficients z_1 and z_2 of the *5snd* $^1D_2$ states in Sr calculated with the MQDT parameters from Ref. [30] and optimized by least square fitting with the experimental hfs – splitting. The errorbars estimate the uncertainty in calculating the mixing coefficients from the MQDT parameters.

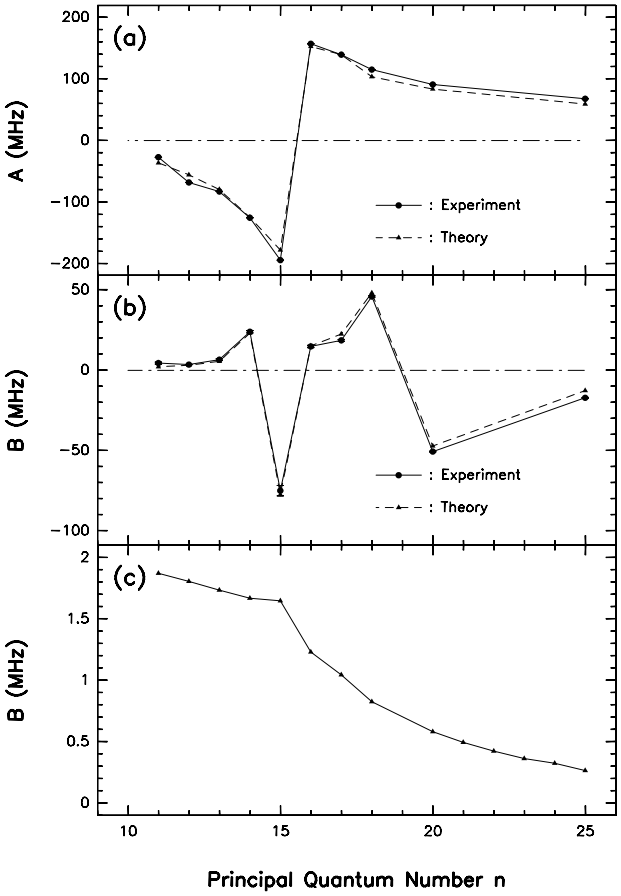

Figure 9: Hyperfine structure constants A and B for the *5snd* $^1D_2$ states in ^{87}Sr as a function of n (see Table 4). In (a) and (b): A and B are determined by fitting the Casimir formula to the measured and calculated line positions. (c): Theoretical prediction for B in first order. It should be noted that the constant B in (b) does not reflect the amount of the electric quadrupole interaction but rather the second order magnetic contribution.

Table 2: Mixing coefficients z_1 and z_2 for the $5snd\ ^1D_2$ Rydberg serie of Sr I (see Eq. (14)) (a) calculated with the MQDT-parameters from Reference [30] and (b) optimized by least square fitting of the theoretical line positions (see also Fig. 8.

	(a)		(b)	
n	z_1	z_2	z_1	z_2
11	0.971(3)	-0.09(2)	0.9732	-0.0651
12	0.966(5)	-0.14(3)	0.9613	-0.1658
13	0.956(2)	-0.195(9)	0.9540	-0.2024
14	0.923(2)	-0.309(6)	0.9226	-0.3111
15	0.86(3)	-0.46(5)	0.8252	-0.5090
16	0.81(4)	0.54(7)	0.7560	0.6174
17	0.88(2)	0.44(3)	0.8771	0.4400
18	0.943(6)	0.29(2)	0.9282	0.3361
20	0.9667(9)	0.220(4)	0.9614	0.2426
25	0.9847(2)	0.152(1)	0.9808	0.1753

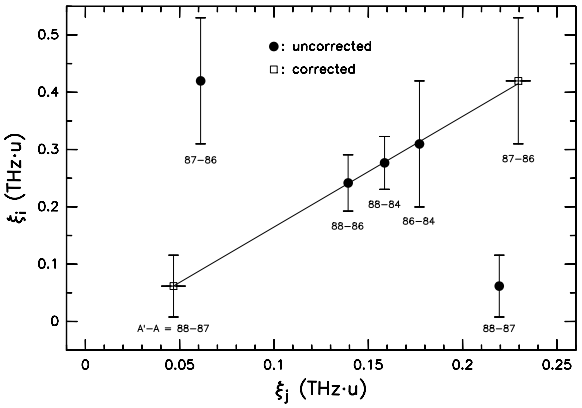

Figure 10: King plot for the two-photon transition j: Sr I $5s^2\ ^1S_0 \rightarrow 5s17d\ ^1D_2$. The values for the reference transition i: Sr II $5s\ ^2S_{1/2} \rightarrow 5p\ ^2P_{1/2}$ are taken from Ref. [39]. The shifts for the isotope pairs involving ^{87}Sr are corrected by an amount given by the center of gravity of the theoretical hyperfine splitting listed in Table 4.

gravity of the theoretical hfs – splitting listed in Table 4 (which is zero without second order effects), the data fit a straight line with excellent agreement.

6 Summary

Higher order contributions to the hfs and to the IS have been studied for ^{87}Sr $5snd\ ^1D_2$ states in the range $11 \leq n \leq 25$. An enhanced accuracy, compared to previous experiments, made it possible to identify second order magnetic dipole contributions to the hyperfine splitting and shift.

In parallel the hfs was calculated in second order pertubation theory using MQDT wavefunctions. We demonstrate that the knowledgement of second order contributions is important for the determination of the quadrupole splitting and the IS, *even* when the fine structure separation is large compared to the hfs – splitting. Neglecting the second order contributions in the hfs analysis of the experimental data leads to unrealistically large quadrupole factors in the Casimir formula as well as to erroneous positions of the centers of gravity which do not give the correct IS.

In the investigated region of n of the $5snd\ ^1D_2$ states, it was shown that the second order magnetic dipole contribution to the hfs – splitting is near $n = 15$ up to one hundred times larger than the first order electric quadrupole contribution which is determined by small admixtures of doubly excited states. Because of the dominance of the second order magnetic dipole contributions it was not possible to make any reliable predictions, based on experimental data, about the admixtures of doubly excited channels into the wavefunction of the $5snd\ ^1D_2$ states that could significantly improve the results of a MQDT-analysis. Evaluating the IS from the ^{87}Sr spectrum, corrected for the second order contributions of the hfs to the shift, leads to a value consistent with a King-plot analysis.

7 Acknowledgements

We like to thank K.-D. Heber and M. A. Khan for helpful discussions and Jun-qiang Sun for his help related to the calculation of the matrix elements.

8 Tables

Table 3: Mean values of the frequency differences with regard to ^{88}Sr for the transitions $5s^2\ ^1S_0 \rightarrow 5snd\ ^1D_2$ of the isotope pairs (^{87}Sr,^{88}Sr), (^{86}Sr,^{88}Sr) and (^{84}Sr,^{88}Sr).

	$\nu^{87} - \nu^{88}$ (MHz)					$\nu^{86} - \nu^{88}$ (MHz)	$\nu^{84} - \nu^{88}$ (MHz)
n	$F = 5/2$	$F = 7/2$	$F = 9/2$	$F = 11/2$	$F = 13/2$		
11	185.83(45)	89.81(25)	-33.67(65)	-179.95(28)	-352.37(29)	-244.99(21)	-511.50(49)
12	634.105(95)	395.214(82)	88.69(12)	-285.218(84)	-724.297(87)	-248.785(57)	-521.06(13)
13	799.25(20)	507.14(42)	133.57(28)	-320.94(25)	-854.17(48)	-240.73(11)	-502.95(26)
14	1268.92(67)	821.63(71)	249.24(23)	-439.12(24)	-1240.48(72)	-241.03(18)	504.66(30)
15	2019.3(11)	1372.1(14)	523.41(80)	-543.91(73)	-	-246.54(83)	-516.71(68)
16	-1844.34(65)	-1299.56(56)	-598.83(26)	267.47(20)	1295.54(66)	-242.60(18)	-508.06(30)
17	-1651.93(67)	-1172.44(47)	-550.56(21)	217.64(27)	1134.18(39)	-234.36(14)	-490.29(15)
18	-1404.38(42)	-1019.48(50)	-511.16(32)	126.10(17)	904.67(26)	-230.05(15)	-481.55(24)
19	-	-	-	-	-	-227.97(25)	-477.05(42)
20	-1054.77(18)	-712.84(23)	-287.75(15)	212.58(14)	777.65(18)	-226.23(14)	-472.68(29)
25	-811.90(20)	-566.69(23)	-255.836(82)	118.212(64)	550.13(21)	-222.179(49)	-464.76(18)

Table 4: A and B constants and centers of gravity for the $5snd\ ^1D_2$ states of ^{87}Sr determined by fitting the Casimir formula to the measured and calculated line positions (see Fig. 9(a) and 9(b). The theoretical line positions are calculated with the mixing coefficients obtained from the MQDT parameters given in Ref. [30]. It should be noted that the isotope shift is not taken into account for the theoretical values $\langle \Delta\nu_F^{87} \rangle$.

	Experiment			Theory		
n	A (MHz)	B (MHz)	$\langle \nu_F^{87} - \nu^{88} \rangle$ (MHz)	A (MHz)	B (MHz)	$\langle \Delta\nu_F^{87} \rangle$ (MHz)
11	-26.855 (20)	4.49 (57)	-111.72 (15)	-36.06	2.2	-4.48
12	-67.895 (57)	3.55 (15)	-114.21 (10)	-55.50	3.2	-6.11
13	-82.605 (26)	6.59 (50)	-112.43 (16)	-79.39	5.6	-7.56
14	-125.217 (37)	24.01 (79)	-119.22 (24)	-124.50	23.1	-13.96
15	-194.02 (18)	-75.0 (32)	-80.70 (99)	-177.56	-77.4	22.74
16	157.248 (34)	14.85 (75)	-121.80 (21)	152.84	15.2	-16.36
17	139.542 (28)	18.64 (61)	-126.13 (17)	139.57	22.5	-22.54
18	115.29 (13)	45.96 (43)	-150.29 (13)	103.66	48.2	-48.68
20	91.067 (11)	-50.62 (25)	-29.50 (10)	83.65	-47.1	71.22
25	67.954 (69)	-17.12 (24)	-56.78 (10)	59.36	-12.6	47.38

9 Hyperfine interaction matrix elements

9.1 Magnetic dipole interaction

$$\langle \ell_1\ell_2 SLJIF|H_\mu|\ell_1\ell_2 S'L'J'IF\rangle = (-1)^{J'+I+F}\sqrt{I(I+1)(2I+1)}\left\{\begin{array}{ccc} J & I & F \\ I & J' & 1 \end{array}\right\}$$
$$\times\,(\ell_1\ell_2 SLJ||\sum_{i=1}^{2} a_{\ell_i}(\boldsymbol{\ell}^{(1)} - \sqrt{10}[\mathbf{s}^{(1)}\times\mathbf{C}^{(2)})]^{(1)} + a_{s_i}\delta_{\ell_i,0}\mathbf{s}^{(1)}||\ell_1\ell_2 S'L'J')\,,$$

$$(\ell_1\ell_2 SLJ||\sum_{i=1}^{2} a_{\ell_i}\boldsymbol{\ell}^{(1)}||\ell_1\ell_2 S'L'J')$$
$$= (-1)^{S+L'+J+\ell_1+\ell_2}\sqrt{(2J+1)(2J'+1)(2L+1)(2L'+1)}\left\{\begin{array}{ccc} L & J & S \\ J' & L' & 1 \end{array}\right\}$$
$$\times\left[\langle a_{\ell_1}\rangle(-1)^{L'}\sqrt{\ell_1(\ell_1+1)(2\ell_1+1)}\left\{\begin{array}{ccc} \ell_1 & L & \ell_2 \\ L' & \ell_1 & 1 \end{array}\right\}\right.$$
$$\left. + \langle a_{\ell_2}\rangle(-1)^{L}\sqrt{\ell_2(\ell_2+1)(2\ell_2+1)}\left\{\begin{array}{ccc} \ell_2 & L & \ell_1 \\ L' & \ell_2 & 1 \end{array}\right\}\right]\delta_{S,S'}\,, \quad (20)$$

$$(\ell_1\ell_2 SLJ||\sum_{i=1}^{2} a_{\ell_i}[\mathbf{s}^{(1)}\times\mathbf{C}^{(2)}]^{(1)}||\ell_1\ell_2 S'L'J')$$
$$= (-1)^{\ell_1+\ell_2}\frac{3}{\sqrt{2}}\sqrt{(2J+1)(2J'+1)(2L+1)(2L'+1)(2S+1)(2S'+1)}\left\{\begin{array}{ccc} \frac{1}{2} & S & \frac{1}{2} \\ S' & \frac{1}{2} & 1 \end{array}\right\}\left\{\begin{array}{ccc} S & S' & 1 \\ L & L' & 2 \\ J & J' & 1 \end{array}\right\}$$
$$\times\left[\langle a_{\ell_1}\rangle(-1)^{S'+L'}(\ell_1||\mathbf{C}^{(2)}||\ell_1)\left\{\begin{array}{ccc} \ell_1 & L & \ell_2 \\ L' & \ell_1 & 2 \end{array}\right\} + \langle a_{\ell_2}\rangle(-1)^{S+L}(\ell_2||\mathbf{C}^{(2)}||\ell_2)\left\{\begin{array}{ccc} \ell_2 & L & \ell_1 \\ L' & \ell_2 & 2 \end{array}\right\}\right], \quad (21)$$

$$(\ell||\mathbf{C}^{(2)}||\ell) = -\sqrt{\frac{\ell(\ell+1)(2\ell+1)}{(2\ell+3)(2\ell-1)}}\,, \quad (22)$$

$$(\ell_1\ell_2 SLJ||\sum_{i=1}^{2} a_{s_i}\delta_{\ell_i,0}\mathbf{s}^{(1)}||\ell_1\ell_2 S'L'J') = (-1)^{S+L+J'+1}\sqrt{\frac{3}{2}}\sqrt{(2J+1)(2J'+1)(2S+1)(2S'+1)}$$
$$\times\left\{\begin{array}{ccc} S & J & L \\ J' & S' & 1 \end{array}\right\}\left\{\begin{array}{ccc} \frac{1}{2} & S & \frac{1}{2} \\ S' & \frac{1}{2} & 1 \end{array}\right\}[(-1)^{S'}\langle a_{s_1}\rangle\delta_{\ell_1,0} + (-1)^{S}\langle a_{s_2}\rangle\delta_{\ell_2,0}]\delta_{L,L'}\,. \quad (23)$$

9.2 Electric quadrupole interaction

$$\langle \ell_1 \ell_2 SLJIF|H_Q|\ell_1 \ell_2 S'L'J'IF\rangle$$
$$= (-1)^{J'+I+F+1}\sqrt{\frac{(2I+3)(2I+1)(I+1)}{4I(2I-1)}}\left\{ \begin{array}{ccc} J & I & F \\ I & J' & 2 \end{array} \right\}(\ell_1 \ell_2 SLJ||e^2Q\sum_{i=1}^{2} r_i^{-3}\mathbf{C}^{(2)}||\ell_1 \ell_2 S'L'J')\,, \quad (24)$$

$$(\ell_1 \ell_2 SLJ||e^2Q\sum_{i=1}^{2} {r_i}^{-3}\mathbf{C}^{(2)}||\ell_1 \ell_2 S'L'J')$$
$$= (-1)^{S+L'+J+\ell_1+\ell_2}\sqrt{(2J+1)(2J'+1)(2L+1)(2L'+1)}\left\{ \begin{array}{ccc} L & J & S \\ J' & L' & 2 \end{array} \right\}$$
$$\times\left[\langle b_{\ell_1}\rangle(-1)^{L'}(\ell_1||\mathbf{C}^{(2)}||\ell_1)\left\{ \begin{array}{ccc} \ell_1 & L & \ell_2 \\ L' & \ell_1 & 2 \end{array} \right\} + \langle b_{\ell_2}\rangle(-1)^{L}(\ell_2||\mathbf{C}^{(2)}||\ell_2)\left\{ \begin{array}{ccc} \ell_2 & L & \ell_1 \\ L' & \ell_2 & 2 \end{array} \right\}\right]\delta_{S,S'}\,. \quad (25)$$

References

[1] M. Aymar, Phys. Rep. **110**, 163 (1984).

[2] E. Matthias *et al.*, *Hyperfine structure and isotope shifts of Rydberg states in alkaline earth atoms* in Atomic Physics 8, edited by I. Lindgren, A. Rosén and S. Svanberg, 543, Plenum Press: New York (1983).

[3] H. Schüler, and E. G. Jones, Z. Phys. **77**, 801 (1932).

[4] H. Casimir, Z. Phys. **77**, 811 (1932).

[5] S. Goudsmit, and R. F. Bacher, Phys. Rev. **43**, 894 (1933).

[6] P. F. Liao, R. R. Freeman, R. Panock, and L. M. Humphrey, Opt. Commun. **34**, 195 (1980).

[7] R. Beigang and A. Timmermann, Phys. Rev. A **25**, 1496 (1982).

[8] R. Beigang, E. Matthias, and A. Timmermann, Z. Phys. A **301**, 93 (1981).

[9] R. Beigang and A. Timmermann, Phys. Rev. A **26**, 2990 (1982).

[10] R. Beigang, D. Schmidt, and A. Timmermann, J. Phys. B **15**, L201 (1982).

[11] P. Grafström *et al.*, Z. Phys. A **306**, 281 (1982).

[12] J. Neukammer and H. Rinneberg, J. Phys. B **15**, 3787 (1982).

[13] J. Neukammer and H. Rinneberg, J. Phys. B **15**, L723 (1982).

[14] E. R. Eliel and W. Hogervorst, J. Phys. B **16**, 1881 (1983).

[15] H. Rinneberg, J. Neukammer, and E. Matthias, Z. Phys. A **306**, 11 (1982).

[16] J. J. Labarthe, J. Phys. B **11**, L1 (1978).

[17] J. Dembczyński, and H. Rebel, Kernforschungszentrum Karlsruhe, Institut für Kernphysik, Report KfK 3606, Nov. 1983, ISSN 0303-4003.

[18] C. S. Kischkel, M. Baumann, and E. Kümmel, J. Phys. B **24**, 4845 (1991).

[19] R. Beigang, W. Makat, A. Timmermann, and P. J. West, Phys. Rev. Lett. **51**, 771 (1983).

[20] Jun-qiang Sun and K. T. Lu, J. Phys. B **21**, 1957 (1988).

[21] Jun-qiang Sun, K. T. Lu, and R. Beigang, J. Phys. B **22**, 2887 (1989).

[22] R. Beigang, E. Matthias, and A. Timmermann, Phys. Rev. Lett. **47**, 326 (1981); **48**, 4 (1982).

[23] C.-J. Lorenzen, K. Niemax, and L. R. Pendrill, Phys. Rev. A **28**, 2051 (1983).

[24] K.–D. Heber, P. J. West, and E. Matthias, Phys. Rev. A **37**, 1438 (1988).

[25] H. Gerhardt *et al.*, Appl. Phys. **22**, 361 (1980).

[26] R. Beigang, W. Makat, and A. Timmermann, Opt. Commun. **49**, 253 (1984).

[27] I. I. Sobel'man, *Introduction to the Theory of Atomic Spectra*, Pergamon Press: Braunschweig (1972).

[28] H. B. G. Casimir, *On the Interaction Between Atomic Nuclei and Electrons*, reprinted by W. H. Freeman, San Francisco (1963).

[29] A. Lurio, M. Mandel, and R. Novick, Phys. Rev. **126**, 1758 (1962).

[30] P. Esherick, Phys. Rev. A **15**, 1920 (1977).

[31] A. Aspect *et al.*, J. Phys. B **17**, 1761 (1984).

[32] M. Aymar, E. Luc–Koenig, and S. Watanabe, J. Phys. B **20**, 4325 (1987).

[33] U. Johann, J. Dembczyński, and W. Ertmer, Z. Phys. A, **303**, 7 (1981).

[34] R. Beigang, and D. Schmidt, Physica Scripta **27**, 172 (1983).

[35] R. Beigang, K. Lücke, A. Timmermann, and P. J. West, Opt. Comm. **42**, 19 (1982).

[36] R. Beigang, K. Lücke, A. Timmermann, and P. J. West, Physica Scripta **26**, 183 (1982).

[37] D. Schmidt, Ph.D. Thesis, Freie Universität Berlin, Germany, 1984.

[38] C. E. Moore, *Atomic Energy Levels*, Nat. Stand. Ref. Data Ser., NBS (U.S. GPO, Washington, D.C., 1952), Vol. 2.

[39] G. Borghs, P. De Bisschop, M. van Hove, and R. E. Silverans, Hyperfine Interactions **15/16**, 177 (1983).

[40] S. M. Heider and G. O. Brink, Phys. Rev. A **16**, 1371 (1977).

[41] C. M. Lederer and V. S. Shirley, *Table of Isotopes*, Wiley & Sons Inc.: New York (1978).

[42] R. Beigang, K. Lücke, and A. Timmermann, Phys. Rev. A **27**, 587 (1983).

[43] K. Heilig and A. Steudel, At. Data Nucl. Data Tables **14**, 613 (1974).